PHILOSOPHICAL TRANSACTIONS OF THE ROYAL SOCIETY B BIOLOGICAL SCIENCES

The Wing Beat of Drosophila Melanogaster. II. Dynamics

J. M. Zanker and K. G. Gotz

Phil. Trans. R. Soc. Lond. B 1990 **327**, 19-44
doi: 10.1098/rstb.1990.0041

Phil. Trans. R. Soc. Lond. B **327**, 19–44 (1990) [19]
Printed in Great Britain

THE WING BEAT OF *DROSOPHILA MELANOGASTER* II. DYNAMICS

BY J. M. ZANKER AND K. G. GÖTZ
Max-Planck-Institut für biologische Kybernetik, Spemannstrasse 38, *D*-7400, *Tübingen, F.R.G.*

(*Communicated by M. F. Land, F.R.S. – Received* 26 *August* 1988)

CONTENTS

The wing beat of tiny insects has attracted considerable interest because conventional aerodynamics predicts a reduction of flight efficiency when aerofoils are comparatively small and slow. Here, two approaches are reported by which we investigated the dynamics of the wing beat of tethered flying *Drosophila melanogaster*. First, the forces acting on the moving wing were calculated from three-dimensional kinematic data, following the blade-element theory which assumes quasi-steady aerodynamics. Under these conditions, the flight force is directed upwards, relative to the longitudinal body axis, during the second half of the downstroke; it is oriented forwards and downwards during the upstroke. The time average of the force generated according to this theory does not correspond to the direction and magnitude of the actual average force of flight. The expected force is directed forwards, along the body's longitudinal axis, and is too small to keep the fly airborne. Secondly, an attempt is made to measure the timecourse of flight forces by attaching the fly to a string, the displacement of which is monitored by means of laser interferometry. A sharp lift-pulse is observed when the wing is rapidly rotated during the ventral reversal of the wing-beat cycle. A second lift maximum of variable strength seems to be associated with the squeeze–peel events during the dorsal reversal. These results

support the notion that flight in small insects might be dominated by unsteady mechanisms.

1. Introduction

Animal flight can be observed in manifold appearances, from the soaring of huge vultures to the hovering flight of tiny insects. Most puzzling is the elaboration of natural flying machines, by which hummingbirds stabilize their position in the air in front of flowers, or dragonflies perform their aerobatic mating dances. The ease and perfection of animal flight challenged human engineers to create flying machines (which mainly impress by their size) and to explain flight capability by simple principles of physics. In the present paper we investigate how far conventional aerodynamic theories can account for the hovering flight performance of small insects. A list of the symbols used in the following equations is given in appendix 1 of the previous report on wing-beat kinematics (Zanker 1990*a*) (paper 1).

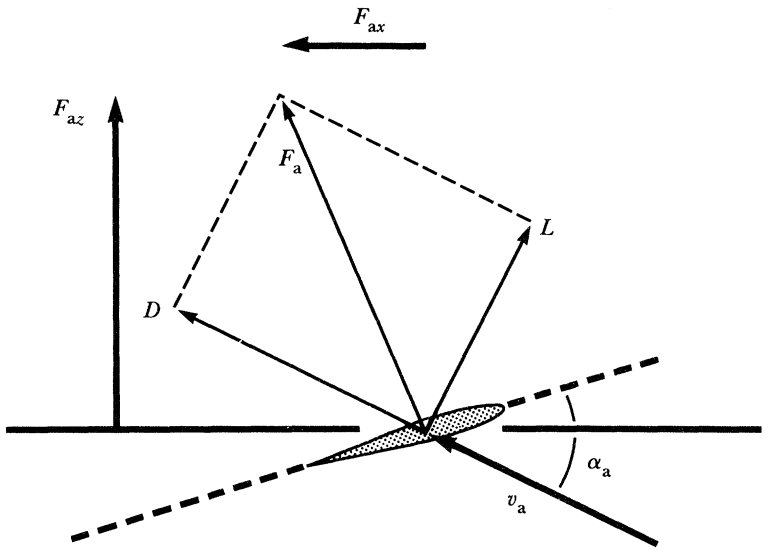

Figure 1. Aerodynamic force. When an aerofoil (profile section shaded) moves relative to the surrounding air at a constant speed v_a and with a constant angle of attack α_a, a drag force D acts on the wing along the direction of motion, and a lift force L normal to D. The resulting flight force vector F_a is decomposed into the horizontal component F_{ax} and the vertical component F_{az} in body coordinates.

The success of man-made flying machines is based on the fact that lift is induced on a wing which is moving at a velocity v_a relative to the surrounding air. The aerodynamic force F_a (figure 1) acting on an aerofoil of length R and chord c is described by two equations for the drag component D, parallel to the direction of relative motion, and the lift component L, normal to the movement direction, respectively (for a more comprehensive description and discussion of stationary aerodynamics, see, for instance, Ellington 1984*a*).

$$L = \tfrac{1}{2}\rho v_a^2 cRC_L; \quad (1)$$

$$D = \tfrac{1}{2}\rho v_a^2 cRC_D. \quad (2)$$

In these equations, ρ is the density of the medium in which the aerofoil is moving. The coefficients of lift and drag, C_L and C_D respectively, depend on the size and shape of the aerofoil

and on the angle under which the wing is hit by the air, the aerodynamic angle of attack α_a. These coefficients are often derived empirically by exposing a particular aerofoil to a defined air stream and measuring the induced forces.

For an aerofoil rotating about an axis, like the blades of a helicopter, or oscillating about a pivot, like the wings of insects, bats or birds,the relative velocity between wing and surrounding medium, v_a, and the aerodynamic angle of attack, α_a, varies from the proximal to the distal end of the wing. The *blade-element theory* (Osborne 1951) takes this into account by dissecting the wing along its span R into infinitesimal blade elements characterized by their width dr and their radial distance r from the axis of rotation. For these elements the equations 1 and 2 are solved by replacing R by dr. The integral over r from 0 to R yields the weighted spatial average of the aerodynamic forces acting on the wing, for a given position during the wing-beat cycle. This oversimplified approach neglects the effects of acceleration and the effects of spanwise components of air flow.

A correction is necessary when applying equations 1 and 2 to insect flight. For the oscillating wing, the velocity of the wing element relative to the surrounding medium is composed of components due to the flapping velocity of the wing v_{flap}, the translational velocity of the animal v_{trans} (which is zero in hovering flight), and the 'induced velocity' v_{ind}. The induced velocity is caused by the downward momentum imparted to the air by the fly, in order to obtain a lift force by reaction. The mean value of the induced velocity can be estimated from the mass of the hovering fly, m_{fly}, and the area covered by the wing stroke, A_s, according to the Rankine–Froude axial momentum theory of propellers (see Osborne 1951):

$$m_{fly}\, g = 2\rho A_s\, v_{ind}^2, \tag{3}$$

with g being the gravitational constant. In the following, the aerodynamic effective velocity, v_a, includes the induced velocity v_{ind} and thus represents a fair approximation of the relative motion between wing and surrounding air.

The ratio between inertial and frictional forces, responsible for the lift and drag component respectively, is reflected by the Reynolds number Re. For a wing element of the characteristic size c, the length of its chord, moving at a speed of v_a, it is given by:

$$Re = cv_a/\nu \tag{4}$$

with ν being the kinematic viscosity of the medium. The investigation of technical aerofoils (Thom & Swart 1940) confirmed that with decreasing Reynolds numbers the lift:drag ratio approaches very small values.

Like common technical aerofoils, most bird wings operate at Reynolds numbers well above 10^4 (Ellington 1984*a*) with a satisfying lift:drag ratio. In contrast, the estimated Reynolds numbers of small insects may fall far below 100, where the frictional forces acting on the wings may exceed the expected lift from the inertial forces. For such insects, effective lift production is particularly difficult to explain by the steady aerodynamics described so far. A sort of 'swimming in the air' was proposed for tiny insects as an alternative mechanism of flight-force production. In this case frictional forces can be utilized when the wing area actually exposed to the air is reduced during the upstroke, compared with the downstroke (Horridge 1956), or when the downstroke is faster than the upstroke (Bennett 1973). This view was challenged by the observation that no kinematic adaptations to such a mechanism can be found in small insects. On the other hand, drag mechanisms seem likely to be involved in the flight of bigger

insects such as butterflies, operating at higher Reynolds numbers (about 3000) (Weis-Fogh 1973; Ellington 1984*a*). For *Drosophila*, the kinematic study reported in Zanker (1990*a*) did not provide any hint of a 'swimming' mechanisms, either.

The most serious problem introduced by the conventional analysis of *Drosophila* aerodynamics is the implicit assumption that the instantaneous forces on the oscillating wing are the same as those for a wing in steady motion at the same velocity and attitude. Whether this *quasi-steady assumption* is justified has been the matter of a long controversy (see Jensen 1956; Weis-Fogh 1973; Ellington 1984*a–d*, for example). Ellington's conclusive rejection of the quasi-steady assumption was based on a proof by contradiction: the mean lift coefficient satisfying the net force balance during flight was estimated from the available kinematic data. For some hovering animals, these values exceed the maximum coefficients known from technical or biological aerofoils. Because the mean forces generated by these animals throughout the wing-beat cycle cannot keep the animal airborne, the assumption on which the calculation was based must be false. However, as Ellington (1984*a*, p. 2) puts it, 'a decisive test can only be accomplished by comparing measured instantaneous wing forces with those predicted by the assumption'.

The purpose of the present paper is to attempt to assess the validity of the quasi-steady assumption by comparison of the calculated with the measured forces. The degree of correspondence between calculation and measurement will show whether this rather simple theory can explain the hovering flight of *Drosophila melanogaster* or whether alternative mechanisms have to be invoked. The following procedure will be applied. (i) Based on the three-dimensional kinematic analysis of tethered flight presented in Zanker (1990*a*, *b*) and the measurement of the wing shape and the lift and drag coefficients, the flight forces are calculated according to the blade-element theory under the quasi-steady assumption. This approach will be called 'quasi-steady theory'. (ii) The timecourse of the forces generated by *Drosophila melanogaster* during fixed flight is measured by the displacement of a string to which the fly is rigidly attached. The comparison of calculated and measured flight forces supports the rejection of quasi-steady theory as an adequate description of the effect of wing beat in *Drosophila*, and leads to (iii) the calculation of some aerodynamic parameters according to the vortex theory (Ellington 1984*d*, *e*).

2. Materials and methods

(*a*) *Kinematic data*

To calculate the forces acting on the wings according to the quasi-steady theory, the velocity v_a and the angle of attack α_a of the wing must be known at any point of the wing and at any time of the wing-beat cycle. These values were derived from the mean kinematic data of *Drosophila* wing-beat cycle reported in paper 1 (Zanker 1990*a*). There, the position and orientation of the wing at 25 phase steps of the wing-beat cycle was approximated by a set of three orthogonal unit vectors which point in the direction of the longitudinal, the transverse and the vertical axis of the wing. The latter vector is normal to the wing surface and attached to the anatomical top side of the wing. By geometric transformations of the axis vectors, α_a and v_a are calculated as a function of time t and radial distance r. All calculations are based on the average kinematic data from 1186 digitized photographs of the two wings from $N = 10$ flies, leading to a mean number of measurements $n = 95$ for each of the 25 phase steps. Use of the

average kinematics saves computation time and reduces the noise which will be blown up by calculating temporal derivatives or geometric transformations. Unfortunately, confidence limits cannot be given under these conditions. However, the extremely low s.e.m.s of the kinematic data shown in paper 1 seemed to justify a simplified procedure. To estimate the s.e.m., the aerodynamic variables are calculated from the individual wing-axis vectors for every phase step; the range and mean of the s.e.ms is given in the figure legends. One should note, however, that these values are only rough estimates, because additional inaccuracies are introduced to the aerodynamic calculations by the limited precision of the morophological wing data (see below).

As mentioned in paper 1, the flies were adjusted with horizontal body axis for technical reasons, although this does not correspond to the natural hovering flight posture with almost horizontal average stroke plane. Thus, the data will be presented in two different coordinate systems. (i) Variables referring to the body axis system (figures 5*a*, *b* and 7) are indicated by the subscripts *x*, *y* and *z*. (ii) To allow for direct comparison of the calculated forces with the forces measured othogonally to the average stroke plane (about 50° inclined relative to the *x*–*y* plane in fly coordinates, see inset in figure 9), the data were finally transformed into a coordinate system referring to the average stroke plane (figure 9), indicated by the subscript s. It has to be emphasized that this purely geometrical transformation seems to be justified, because in tethered flight of *Drosophila* no significant influence of the gravitational vector orientation on flight-force production could be detected (Götz 1968; cf. paper 1).

(*b*) *Wing data*

The blade-element theory requires, in addition to the kinematic data, that the wing chord *c* is known as a function of radial distance *r*. The shape of *Drosophila* wings was evaluated by means of a simple planimetric procedure. A wing was cut at its base and spread on a microscope slide. The outline of the wing was drawn on a sheet of paper, enlarged with a projection microscope by a factor of 100. The length *R* of the wing span was measured from the drawing, and the wing was divided along the longitudinal axis into 20 equidistant sections. Then the chord lengths *c*(*r*) of these 20 sections were determined. The average shape of six wings is

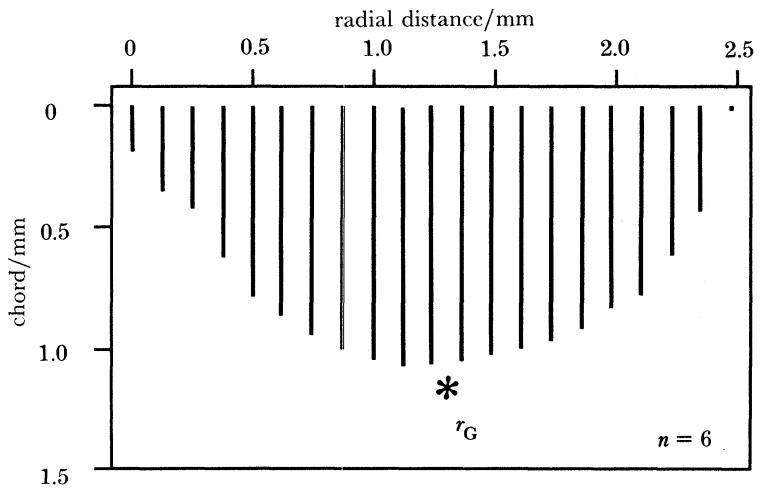

FIGURE 2. Wing shape. Chord length *c* plotted as a function of radial distance *r* from wing base. The asterisk marks the radial distance r_G of the wing's centre of mass. Average values from six planimetrically evaluated wings.

PHILOSOPHICAL TRANSACTIONS OF THE ROYAL SOCIETY B BIOLOGICAL SCIENCES

displayed in figure 2; the radial distance r is transformed back from the section number to its metric dimension, using actual wing lengths. From the wing length $R = 2.47 \times 10^{-3}$ m ($\pm 0.02 \times 10^{-3}$ s.e.m.) and the average wing chord $\bar{c} = 0.85 \times 10^{-3}$ m ($\pm 0.01 \times 10^{-3}$ m s.e.m.), the wing area $A_w = 2.18 \times 10^{-6}$ m^2 ($\pm 0.02 \times 10^{-6}$ m^2 s.e.m.) was determined. These values differ from those published by Curtsinger & Laurie-Ahlberg (1981, 1985) for male *Drosophila melanogaster*, which are generally smaller than the females used in the present study. The radial distance of the wing's centre of gravity, $r_G = 1.25 \times 10^{-3}$ m, was found by calculating the average radial distance, weighted with the respective chord length. Strictly speaking, r_G corresponds to the centroid of the area, which coincides with the centre of gravity (centroid of mass), when thickness and density are virtually constant over the wing. Comparing the data presented by Ellington (Table 1 in 1984*b*) for the centroid of area and the centre of gravity, it is clear that the radial distance of the latter is overestimated by the radial distance of the former, probably because of a distal decrease of the wing's thickness. On the other hand, r_G might be underestimated when the wings were cut slightly distal to its kinematic base. Thus the following calculations will be based on the value of $r_G = 1.25 \times 10^{-3}$ m.

To determine the inertial forces acting during wing accelerations on the thorax, the 'total' mass of the wing, m_{wg}, i.e. the mass of the wing plus the 'virtual' mass of the air accelerated together with the wing, must be known. Twenty wings were cut off the thorax and put on an analysis balance, taking care that weight losses due to evaporation were reduced. The average mass per wing was roughly 5 µg. This corresponds to a value which can be estimated from the wing area A_w, when a mean thickness of the wing of 2×10^{-6} m (i.e. about 0.08 % of R) and a specific density of roughly 1.1×10^3 kg m^{-3} is assumed. In addition, the mass of the air surrounding the wing has to be regarded because this 'virtual' mass is accelerated together with the wing (Alexander & Goldspink 1977; Vogel 1981). Assuming an air cylinder of the mean diameter $\bar{c}$ (Ellington 1984*b*), the virtual mass can be estimated roughly to be 2 µg. Thus the total mass of the wing, m_{wg}, amounts to about 7 µg.

Finally, the lift and drag coefficients C_L and C_D in equations 1 and 2 must be known for the calculation of the flight forces. The conventional procedure to determine the dependence of C_L and C_D on the angle of attack α_a, the 'polar diagrams', is to expose an aerofoil to a laminar flow at a constant velocity v_a. Then α_a is varied and the forces acting on the aerofoil parallel and normal to the flow, D and L, are measured. Here, a similar method was adopted. A *Drosophila* wing was attached axially to a thin steel pin and positioned in the centre of a wind tunnel which produced a laminar air stream. A uniform wind speed of about 1.5 m s^{-1} was maintained within the section of the tunnel to which the wing was exposed. Under the influence of the wind, the steel pin is expected to bend proportionally to the forces acting on the wing. The displacement of the wire was measured by projecting its shadow eccentrically on the aperture of a light sensor. To correct for possible elastic anisotropies of the wire, the measurements were calibrated, for each angle α_a, by placing a small weight on the tip of the pin, near the wing base. From five readings ((i) reference position of the wire without weight in still air; (ii) with 1 mg weight in still air; (iii) reference position as in (i); (iv) without weight in wind; (v) reference position as in (i)) the force acting on the wing and the wire are determined in milligram units for wing inclinations α_a between $-90°$ and $+90°$. When this was accomplished, the wing was detached from the wire and the same procedure was repeated for the wire without the wing. These values were subtracted from the former ones, leading to better estimates for the forces resulting form the wing's aerodynamic properties. In two

separate sets of measurements the lift and drag component of the aerodynamic force were determined by rotating the setup by 90° around an axis perpendicular to the axis of the wind tunnel.

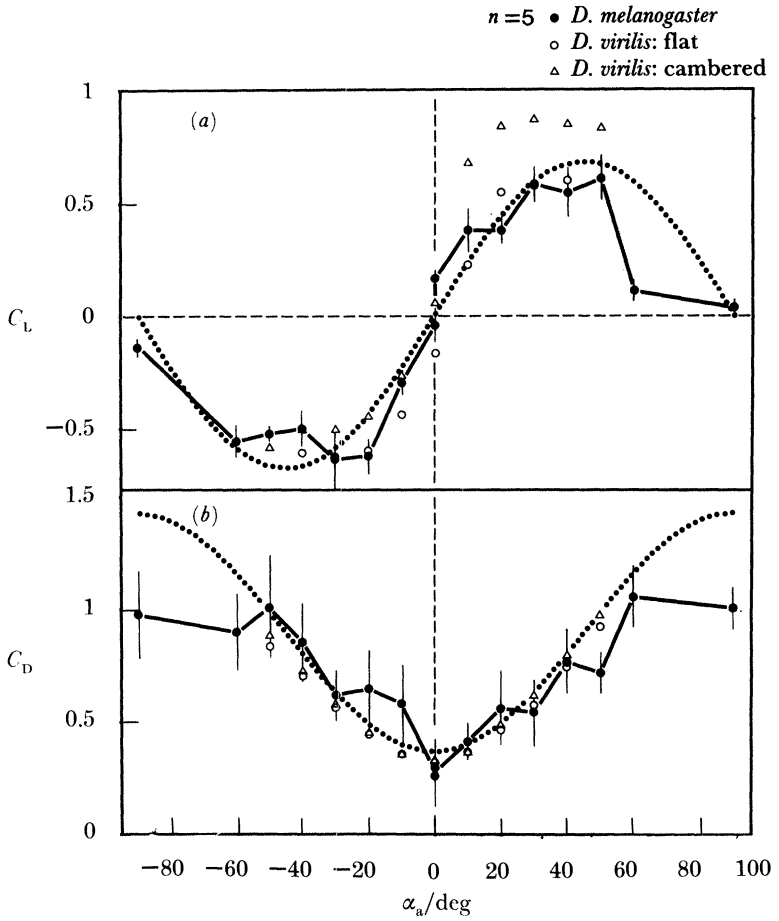

FIGURE 3. Resolved polars of *Drosophila* wings. The aerodynamic coefficient of lift C_L (*a*) and drag C_D (*b*) are plotted as functions of the aerodynamic angle of attack α_a. For aerodynamic calculations, the average values measured from five wings of *Drosophila melanogaster* (black dots; bars denote the s.e.m.) are either interpolated (continuous lines) or approximated by trigonometric functions (dotted lines): $C_L = 0.7 \sin 2\alpha$; $C_D = 0.9–0.5 \cos 2\alpha$. For comparison, the values measured by Vogel (1967) for flat and cambered wings of *Drosophila virilis* are plotted as open circles and triangles, respectively.

The results obtained by this method were not expected to be extremely accurate. Indeed, the average coefficients from five wings presented in figure 3 as 'resolved polars' (black dots; the bars show the standard errors of the mean) do exhibit some scatter. However, the measurements are in qualitative agreement with earlier data published by Vogel (1967) for the larger species *Drosophila virilis* (open symbols in figure 3). The coefficient of drag C_D (bottom panel of figure 3) has a minimum for small inclinations (about 0.4 at $\alpha_a = 0°$) and increases to a maximum of roughly 1.0 for large inclinations ($\alpha_a = \pm 90°$), i.e. the friction slightly increases when the profile area exposed to the airstream is increased. As expected, the coefficient of lift C_L is close to zero at inclinations of 0° or ±90°, i.e. when the wing is exposed symmetrically to the air stream. It reaches values of about +0.5 (−0.5) for α_a between 30° and 60° (−30° and −60°). This means that comparatively strong lift pointing upwards (downwards) is induced, as soon as the wing is inclined nose up (down) relative to the wind.

To allow for the calculation of the aerodynamic forces for any angle of attack, two procedures were followed: either the values were interpolated between the measured coefficients, as indicated by the continuous lines in figure 3, or the polar diagrams were approximated, within reasonable limits for α_a, by simple trigonometric functions, as indicated by the dotted lines and the formulae given in the legend.

(*c*) *Force measurements*

The forces produced during tethered flight have been measured in several insects, by means of a variety of flight balances (see, for example, Hollick 1940; Weis-Fogh 1956; Vogel 1966; Götz 1968; Zarnack 1969; Cloupeau *et al.* 1979; Nachtigall & Roth 1983). Most of these systems were designed to investigate average flight performance. Accordingly, their time resolution was too small to monitor the variations of the flight force during the wing-beat cycle. A technique to record the instantaneous flight forces of *Sarcophaga* was developed by Buckholz (1981). The measurement of the forces instantaneously generated by *Drosophila* during the wing-beat cycle demands a particularly sensitive and fast device, because these forces are very small (the mass of the fly is about 1 mg) and vary with the wing-beat frequency of approximately 200 Hz. Because no conventional balance solves this measuring problem, we developed a special apparatus (sketched in figure 4), based on the taut-wire technique introduced by Buckholz (1981). Basically, the fly is attached to a string, which is tuned to a high resonance frequency. In our experimental setup, the displacement of the string monitoring the instantaneous flight force is recorded by means of laser interferometry.

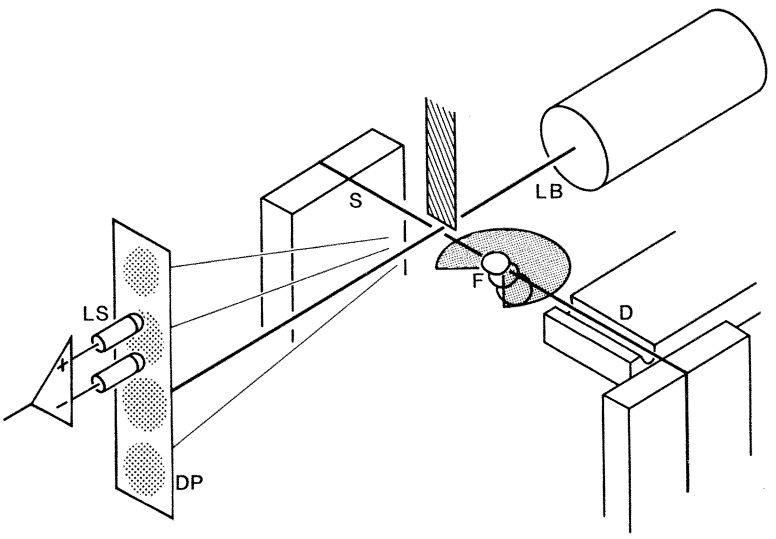

FIGURE 4. Flight force measuring device. A flying *Drosophila* (F) is glued to a string (S), which is damped by a viscous medium in a surrounding groove (D). The width of a horizontal gap between the string and a complementary strip of metal lowered from above is varied according to the force of flight. This changes the distance of the fringes in the diffraction pattern (DP) of a laser beam (LB). The analogue signal of a differential light sensor (LS) positioned at the flanks of the first fringe monitors the instantaneous displacement of the string.

In all experiments, female wild-type *Drosophila melanogaster*, 3–8 days old, from the laboratory stock 'Berlin' were used. Under cold anaesthesia they were glued with their head and thorax to the string. As soon as the fixed fly recovers from the anaesthesia, it starts flying. Care was taken to adjust the body axis such that the average stroke plane was approximately horizontal, just as during hovering flight. The major advantage of a horizontal stroke plane is

the reduction of inertial force components in the force signal measured orthogonally to this plane. In this case, they are limited to the effects of the wing leaving the average stroke plane. By increasing its tension, the steel string (diameter 0.15 mm, length 45 mm) was tuned to a resonance frequency between 2 and 5 kHz. To prevent continuous oscillations at resonance frequency after sharp and/or repeated excitations of the string, it had to be damped. A mixture of vaseline and paraffin oil was used to fill a small groove around the string (D in figure 4). The viscosity of this mixture was adapted to approximate critical damping. However, when a small weight was dropped on the string, the induced oscillation was damped to about 5% after five oscillation periods, or 2×10^{-3} s, in a typical case. This corresponds to a logarithmic decrement of 0.6. The string displacements thus reflect both the flight forces produced by the fly, and the resonance properties of the string.

Owing to the strong tension on the string, the displacement induced by the flight forces were extremely small. To measure these displacements a laser beam was sent through the small gap between the string and the parallel edge of a plate held by a microdrive (figure 4). When the gap was narrow enough, an interference pattern was displayed on a screen placed at 0.7 m from the string. The basic distance between neighbouring maxima of the interference pattern was set by adjusting the width of the gap. When the string moved, the width of the gap was slightly varied and the fringes of the diffraction pattern were shifted correspondingly. The displacement of the fringes could be simply recorded by a light sensor. The signal : noise ratio was improved by a differential input system with the two sensors focused on the opposing flanks of the first fringe of the diffraction pattern. This device is insensitive to fluctuations of background light. Throughout the experiments, the displacement of the string was very small in comparison to its length, and the resulting displacements of the maxima very small in comparison to the distance between the maxima of adjacent fringes in the diffraction pattern. This justifies the assumption of a linear relation between the analogue signal of the differential light sensor and the external and internal forces acting on the string.

Because the actual properties of the described apparatus depended on the tension, the attached weight, the damping conditions and the position of the light sensor relative to the diffraction pattern, a calibration was required for every experiment. A complete frequency characteristic was too complicated and time-consuming to be determined; thus (i) the sign of the signal was verified by pressing a hair-like wire on the string from above and from below; and (ii) the resonance properties were controlled qualitatively by dropping a small weight on the string, which led to damped oscillations.

The experiments and the crude calibrations were recorded on analogue tape (RACAL store D7) for further analysis. Besides the string displacement, the output of a light barrier positioned over the ventral area of the wing-beat envelope (not shown in figure 4) was recorded. This signal indicates the relative phase of the ventral reversal during the wing-beat cycle. By triggering strobe flashes from this signal, the various kinematic events were assigned, in their relative phase, to the force signal. From the tape, flight sequences of 0.125 s duration (containing about 25 wing-beat cycles) were digitized at a sampling rate of 20 kHz (IBM AT, DT 2818). For further treatment, 20 cycles of a particular flight episode were averaged on a non-dimensional timescale as follows. The time period between two consecutive ventral wing-beat reversals determines a single wing-beat cycle. This period was divided into 100 equidistant phase intervals of the wing-beat cycle. The signals from 20 wing-beat cycles were collected and averaged for each of these intervals. This allows presentation of the force measurements

PHILOSOPHICAL TRANSACTIONS OF THE ROYAL SOCIETY B BIOLOGICAL SCIENCES

independently of the actual wing-beat frequency and calculation of the average of the results from different flight episodes and different flies. Because of their non-dimensional timescale, these averages are directly comparable to the kinematic data shown in paper 1 (Zanker 1989*a*).

3. Results

(*a*) *Wing velocities*

The relative velocity v_a between the wing and the surrounding air is determined by three factors: (i) the translational velocity of the fly v_{trans}, which is zero in hovering flight; (ii) the flapping velocity v_{flap} of the oscillating wing; (iii) the induced velocity v_{ind} required to obtain equilibrium according to the Rankine–Froude momentum theory (equation 3). For hovering flight, the average induced velocity $v_{ind} = 0.51$ m s^{-1} results from the fly's mass $m_{fly} \approx 1 \times 10^{-3}$ g and an estimated wing-stroke area $A_s = 14 \times 10^{-6}$ m^2 (2.5×10^{-3} m long wings beating over an average stroke amplitude of 135°). This value of v_{ind} is not negligible compared with the wings' flapping velocity $v_{flap} < 2.5$ m s^{-1} or the fly's forward velocity $v_{trans} < 1$ m s^{-1} under the conditions of free flight (David 1978). Two points have to be considered before using v_{ind} for further calculations. (i) The induced velocity was calculated from the force balance for hovering flight, which corresponds to the experimental situation without external wind. In that case the average stroke plane would be roughly horizontal (cf. Weis-Fogh 1972), i.e. the body axis would be about 50° inclined relative to the horizontal plane (David 1978; Zanker 1988). Thus, the angle between the vector representing v_{ind} and the fly's body axis is about −140°, because the air flow is assumed to be directed downwards (see inset in figure 9). This inclination of v_{ind} relative to the fly's longitudinal axis leads to a horizontal component of 0.39 m s^{-1} and vertical component of 0.33 m s^{-1} in body coordinates. (ii) It should be noted that in our crude approximation the induced velocity was assumed to be equally distributed over the wing-stroke area. It neglects spatial and temporal variations due to the relative movement of the rapidly oscillating wings (see Wood 1970) and may therefore locally underestimate the relative velocity between the wing and the surrounding air. However, in the light of serious inherent simplifications of the quasi-steady theory, this first approximation appeared tolerable.

The velocity components resulting from the wing oscillation were calculated from the kinematic data presented in paper 1 (Zanker 1989*a*). The translational velocity of the wing was derived by dividing the difference of the wing positions before and after a particular phase step by the time interval corresponding to two of the 25 phase steps per wing-beat cycle, or $2/(25\, n_f)$. The average, n_f, of the actual wing-beat frequencies of the ten flies was 202 s^{-1}, with a standard error of the mean of ±2.8 s^{-1}. The horizontal and vertical wind component in the sagittal plane of the fly, v_x and v_z, are plotted in figure 5 (*a*, *b*). As expected from the wing path, the horizontal velocity v_x is positive (negative) and the vertical velocity v_z is negative (positive) during downstroke (upstroke). Because the absolute size of the resulting velocity v varies considerably from the proximal ($v = v_{ind}$) to the distal end of the wing, the calculated aerodynamic variables will depend strongly on the radial distance r.

Finally, the velocity vector of relative wing motion in body coordinate system (v_x, v_y, y_z) is decomposed into two components (figure 5*c*). (i) The aerodynamic effective velocity v_a is the component in the plane defined by the wing's vertical and transverse axis. Again, this value varies from the proximal to the distal end of the wing; the weighted average along the wing

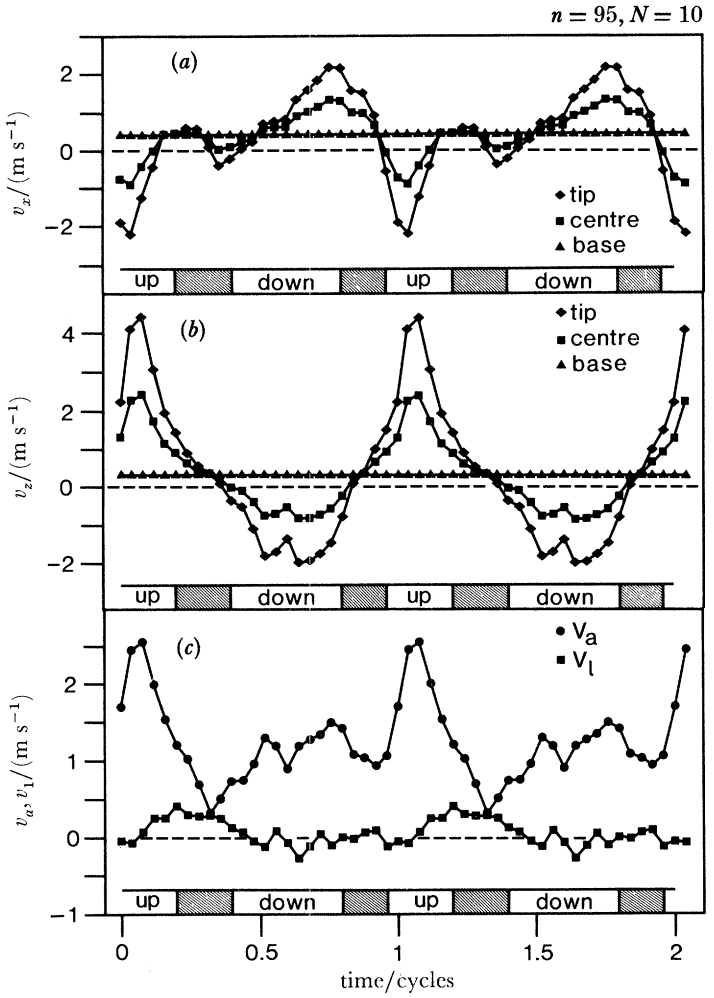

FIGURE 5. Wing velocities. (*a*, *b*) The velocity components along the horizontal (v_x) and vertical (v_z) body axes as functions of time given in fractions of the wing-beat period. Note the increase in the velocity maxima from the base (triangles) to the centre (squares) and the tip (diamonds) of the wing. The wing moves backwards during the upstroke and forwards during the downstroke. The vertical speed shows a distinct maximum during upstroke and a minimum during downstroke. (*c*) The velocity of the wing can be decomposed by appropriate geometric transformations into the aerodynamically efficient component v_a (dots) and a spanwise component v_l (squares), which is small compared with v_a. Data from the kinematic study in paper 1 (*n*, number of evaluated cycles; *N*, number of flies; standard errors of the mean range between ± 0.02 m s^{-1} and ± 0.18 m s^{-1}, their averages are ± 0.07, ± 0.09, ± 0.08 and ± 0.07 m s^{-1} for centre v_x, centre v_z, v_a and v_l, respectively).

span is plotted. It reaches a conspicuous maximum during the upstroke. (ii) The 'longitudinal' velocity component v_l along the wing span is not regarded by the quasi-steady theory. This seems to be justified since the values of v_l are small compared with those of v_a. Note, however, that this conclusion is based on the Rankine–Froude assumption that the induced velocity is essentially normal to the average stroke plane and no additional spanwise components are induced.

Knowing the aerodynamic velocity of the wing, the Reynolds number *Re* of *Drosophila melanogaster* can be estimated according to equation 4. Based on the average chord length $\bar{c} = 0.85 \times 10^{-3}$ m as characteristic length and the average speed $\overline{v_a} = 1.25$ m s^{-1}, the Reynolds number amounts to 80.

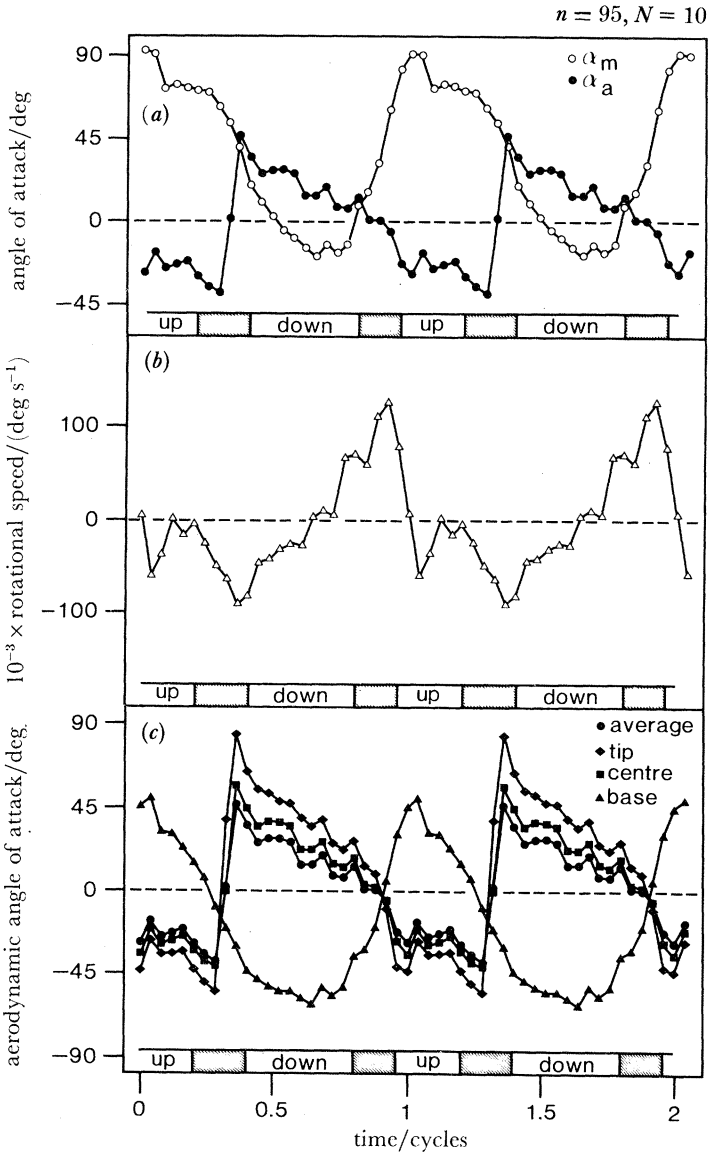

FIGURE 6. Angles of attack. (*a*) Timecourse of both the morphological angle of attack α_m (open circles) and the average aerodynamic angle of attack α_a (black dots). The standard errors of the mean of α_m (α_a) range between $\pm 2.0°$ and $\pm 7.6°$ ($\pm 3.6°$ and $\pm 6.3°$), being $\pm 4.1°$ ($\pm 4.9°$) on average. The angle α_m is positive, i.e. the wing moves leading edge up, except during the downstroke where the wing moves leading edge down ($\alpha_m < 0$). In contrast, α_a is positive during the downstroke, i.e. the wing is touched by the air from below. During the upstroke α_a is negative. (*b*) Time course of the wing's rotational speed about a longitudinal axis, exceeding 10^5 deg s^{-1} during the lower reversal phase (s.e.m.s range between ± 5 and $\pm 21 \times 10^3$ deg s^{-1}, $\pm 12 \times 10^3$ deg s^{-1} on average). (*c*) Timecourse of the aerodynamic angle of attack α_a at various distances from the wing base. Note that the sign of α_a at the wing base (triangles) is opposite to the sign for the distance corresponding to the average (dots), centre (squares) or tip (diamonds) of the wing, respectively. (Data and timescale as in figure 5.)

(*b*) *Angles of attack*

When the wing is oscillating up and down, it is simultaneously rotated about its longitudinal axis: during the downstroke the leading edge is lowered relative to the trailing edge (pronation) whereas during the upstroke it is lifted (supination). These cyclic changes of the

wing's inclination are accomplished mainly during the complicated *squeeze–peel* at the dorsal end of the half-stroke and the *quick rotation* at the ventral end of the half-stroke (see paper 1). Correspondingly, the morphological angle of attack α_m varies between small negative values during the downstroke and high positive values during the upstroke (figure 6*a*). The rotational speed of the wing about its longitudinal axis, $d\alpha_m/dt$, which reflects the performance of the wing joint, reaches extreme values of at least 10^5 deg s^{-1} (figure 6*b*). Jitter in the timecourse of the rotational speed impairs the preservation of the peak in the averaged data. Actual peak amplitudes are likely to exceed the maximum shown in figure 6*b*.

The aerodynamic angle of attack α_a (figure 6*c*) is the angle of the wing relative to the air flow. It is calculated as the angle between the direction of the aerodynamically effective velocity v_a (see above) and the transverse wing axis, in the plane defined by the transverse and vertical wing axes. Because α_a depends both on the morphological angle of attack α_m and on the magnitude and orientation of relative wing motion v_a, the timecourse of α_a varies with the distance r from the wing base to the wing tip. It differs considerably from the time course of α_m for the distal wing areas where the flapping velocity is large in comparison to the induced velocity (figure 6*a*, *c*). The blade-element theory takes this into account by calculating the aerodynamic variables for small wing sections and weighting the result with the area of the given wing element. The timecourse of α_a, calculated as weighted average, at the wing base ($r = 0$), at the wing tip ($r = R$) and the centre of gravity ($r = r_G$) is plotted in figure 6 (*a*, *c*) (black dots). During the downstroke, α_a is positive: the air flow touches the wing from the anatomical bottom side. An enhancement of lift due to Kramer's effect (delay of the stall expected on transition to critically increased angles of attack) (see Ellington 1984*d*) cannot be expected for the downstroke because α_a is continuously decreasing during this period. Throughout the upstroke, α_a is negative: the air flow hits the wing under almost constant angle from its anatomical top side. The trajectory of the wing shown in figure 5 of paper 1 (Zanker 1990*a*) illustrates, qualitatively, the non-intuitive succession of positive and negative angles of attack.

(*c*) *Quasi-steady forces*

From the coefficients of lift, C_L, and drag, C_D of the *Drosophila* wings, the aerodynamic angle of attack α_a and the aerodynamic effective velocity v_a, the lift L and drag D acting on a pair of wings according to the quasi-steady theory were calculated as a function of time t and radial distance r. Depending on the posture of the wings in space the resulting aerodynamic force F_a was decomposed into the three orthogonal components of a fly-centred coordinate system, F_{ax}, F_{ay} and F_{az}. The time course of the two components in the fly's sagittal plane, F_{ax} and F_{az}, is shown in figure 7 (*a*, *b*). Because bilateral symmetry was assumed for the unstimulated fly, the transversal components F_{ay} of the two wings annihilate each other. Mainly owing to the increased flapping velocity, the forces are considerably stronger at the wing tip (black diamonds in figure 7) than at the wing base (black triangles in figure 7). The weighted average according to the blade-element theory (black dots in figure 7) is very close to the value derived by generalization of the flight force calculated for the wing elements at the centre of gravity (black squares in figure 7).

From the kinematic analysis of *Phormia* wing beat during tethered flight in a head wind, Nachtigall (1966) concluded that the fly generates a net flight force along the vertical body axis (which he called 'lift' because the body axis was almost horizontal in his experiments) during the downstroke, and a net force along the longitudinal body axis ('thrust') during the

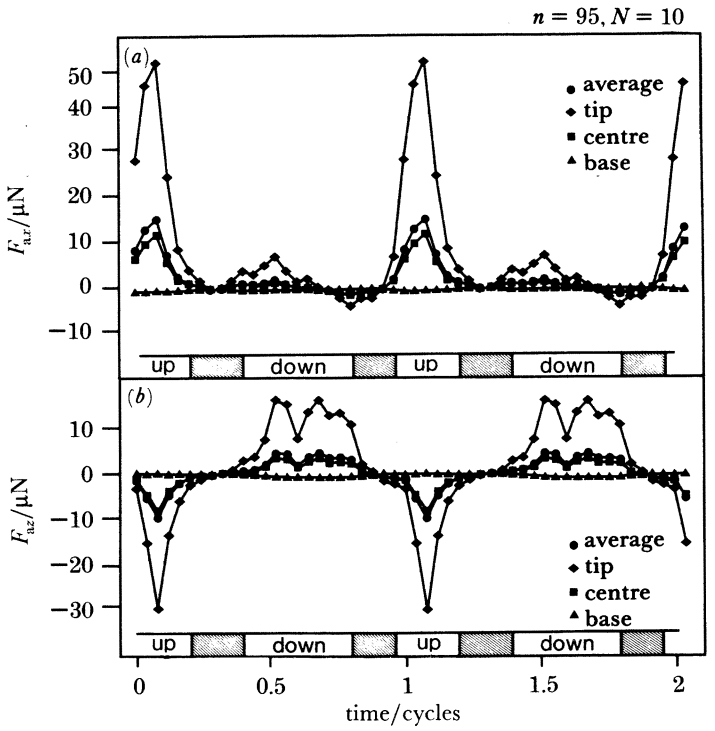

FIGURE 7. Quasi-steady aerodynamic forces. The horizontal (*a*) and vertical (*b*) components of flight forces, F_{ax} and F_{az}, calculated according to the quasi-steady theory for a pair of wings (in body coordinates), are plotted as a function of time. (Data and timescale as figure 5.) The standard errors of the mean range between ±0.28 μN and ±2.48 μN for the weighted averages of F_{ax} (black dots), and between ±0.12 μN and ±1.58 μN for F_{az}. Mean s.e.m.s are ±0.66 μN and ±0.72 μN. Note the variation of the maximum from base (triangles) to tip (diamonds) of the wing. The forces generated during the downstroke act predominantly in upward directions. The forces expected during the upstroke are directed downwards and forwards.

upstroke. However, in *Drosophila* the force production seems to be more complicated. The vertical component F_{az} shows a broad maximum during the second half of the downstroke and a sharp minimum during the upstroke where the forces are directed downwards. The time course of the horizontal component F_{ax} is dominated by a sharp maximum during the upstroke. This discrepancy has to be discussed in the light of the different experimental conditions. In our experiments, the fly was suspended horizontally in still air, which mimics hovering flight with respect to the external wind but not with respect to the fly's body angle (0° instead of 50°). This means that in *Drosophila* F_{az} is not the force component counteracting the animal's weight and F_{ax} is not the force component responsible for thrust. Because the flight force production during tethered flight is almost independent of the fly's orientation in space (see paper 1), hovering flight lift (referring to gravity coordinate system) can be derived by simple geometric transformations of F_{az} and F_{ax}. These data are presented in figure 9, in immediate comparison with the actual measurements of the same force component. On the other hand, one could argue that the additional head wind in Nachtigall's (1966) experiments is crucial for the discrepancy in the orientation of the flight force vector during upstroke and downstroke, respectively. In paper 3 of the present study (Zanker 1990*b*) it will be shown that the basic results are not affected by external wind generated in a wind tunnel.

The present data have been used to average, under various boundary conditions, the flight

TABLE 1. AVERAGE FLIGHT FORCES FOR A WING-BEAT CYCLE

(Forces calculated according to quasi-steady theories by using the kinematic variables found either at the centre of the wings (centre) or by integration over the wing span (integr.) according to the blade-element theory. The aerodynamic coefficients for drag and lift of the two wings were derived from measurements on *Drosophila melanogaster* or *Drosophila virilis*, either by interpolation (interpol.) or by approximation (approx.) with the simple trigonometric functions shown in figure 3.)

			force vectors	
			magnitude	inclination
calculation method	*Drosophila* species	coefficients fitted by	μN	deg
centre	*melanogaster*	appox.	1.34	0
integr.	*melanogaster*	approx.	1.92	6.0
centre	*melanogaster*	interpol.	1.48	−3.9
integr.	*melanogaster*	interpol.	1.88	−0.6
measured	*melanogaster*	—	*4.5*	*24.0*
centre	*virilis*	interpol.	1.92	17.7
integr.	*virilis*	interpol.	2.48	18.9

force over a complete wing beat cycle. The resulting magnitude of the *average flight force vector* F_a (produced by a pair of wings) and its inclination relative to the longitudinal body axis is summarized in table 1. The values of F_a calculated under the assumption that wing action is represented by the kinematics near its centre of gravity (rows 1, 3 and 6 in table 1) are about 25% smaller than those calculated as weighted average over the wing span. Thus the integration over the contributions of blade-elements seems to correct for underestimations of simplified assumptions. As would be expected, however, neither the magnitude nor the inclination of the average force vector is strongly influenced by the application of either interpolated or approximated resolved polars of the wing. When the average flight force is calculated with the aerodynamic coefficients measured by Vogel (1967) for the wings of the larger species, *Drosophila virilis*, F_a is slightly increased and oriented upwards (rows 6 and 7 in table 1), compared with the calculations based on the aerodynamic coefficients measured here for *D. melanogaster* (rows 1–4 in table 1). This result is due to Vogel's slightly increased values of C_L for positive angles of attack (figure 3) when the wing was cambered. It seems to be appropriate to describe the aerodynamics of the smaller species *Drosophila melanogaster* by using the polar diagrams crudely measured for this species here, instead of by using the data from *Drosophila virilis* (twice as heavy), because no indication of any considerable camber could be seen in the slow-motion pictures of *Drosophila melanogaster* wing beat (see Zanker 1990*a*). The inaccuracy introduced by the choice does not change the principle results. In the best case (row 2 in table 1), the flight force amounts to 1.9 μN and is oriented 6° upwards. This is much smaller than the average flight force measured for fixed flying *Drosophila melanogaster* (row 5 in table 1), which amounts to about 4.5 μN (Götz 1987) and is oriented 24° in an upward direction relative to the body axis (Götz & Wandel 1984). This measured average force meets the expected orientation, which should be about normal to the average stroke plane.

(*d*) *Measured forces*

To investigate the time course of force production during the wing-beat cycle, the fly was attached to a steel wire, as described above. The timecourse of the string displacement for three flight episodes, each of 15 ms duration, is presented in figure 8 (*b–d*). The arrows mark the time

PHILOSOPHICAL TRANSACTIONS OF THE ROYAL SOCIETY B BIOLOGICAL SCIENCES

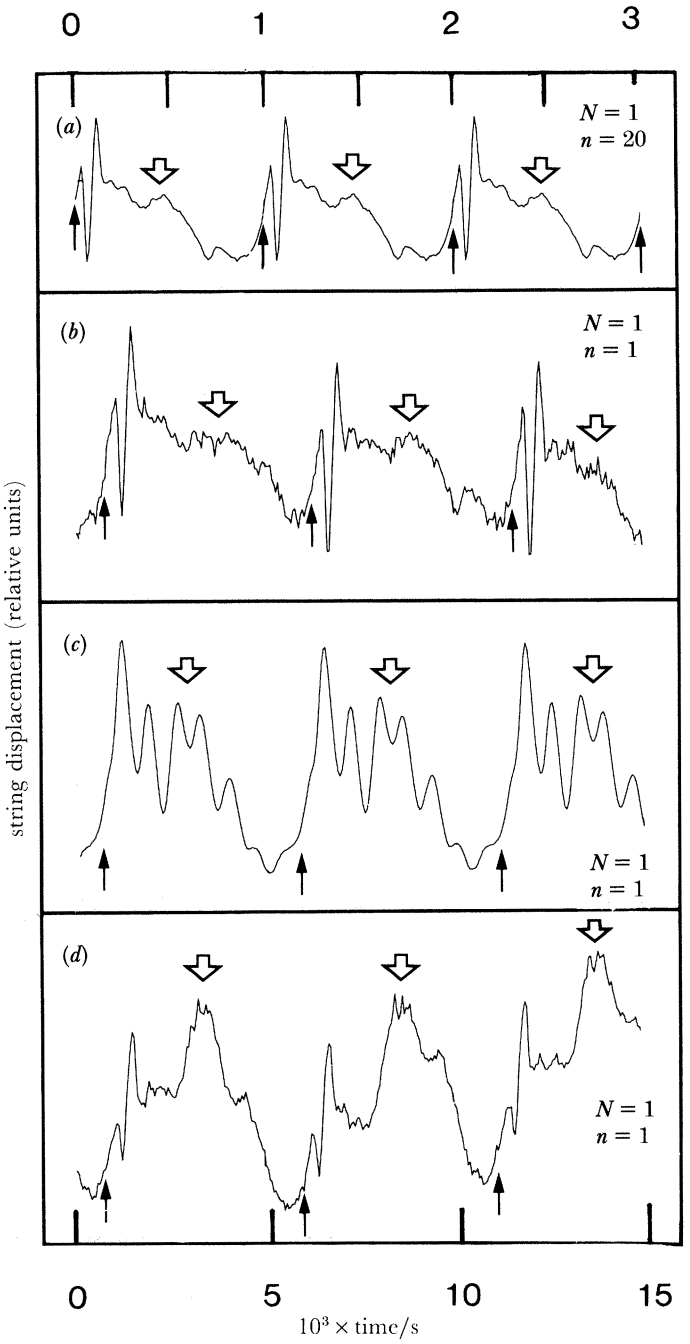

FIGURE 8. Measured flight forces. (*b*) Example of a flight force measurement from a flight episode at a wing-beat frequency of 185 Hz and a string resonance frequency of 3.3 kHz, plotted on the original time scale (bottom). (*a*) Average of 20 wing beat cycles of the same fly plotted on a non-dimensional timescale (top). For comparison the resulting curve has been repeated three times. (*c*, *d*) Two examples from another fly, flying at 189 Hz wing-beat frequency. The resonance frequency was changed from 1.5 kHz (*c*) to 4.5 kHz (*d*). In all cases, there is a strong and instantaneous excitation of the string occurring between downstroke and upstroke (indicated by the black arrows) when the wings are rapidly rotating about their longitudinal axes. A second lift maximum of variable amplitude appears about half a wing-beat cycle later (open arrows).

PHILOSOPHICAL TRANSACTIONS OF THE ROYAL SOCIETY B BIOLOGICAL SCIENCES

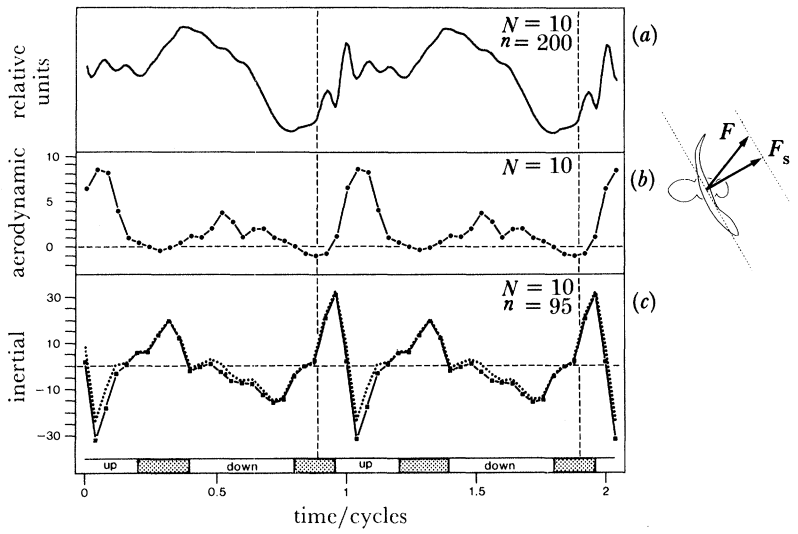

FIGURE 9. Measured and calculated force component F_s perpendicular to the average stroke plane (the reconstruction from the force components in body coordinates is sketched in the inset). (*a*) Average forces measured during 200 wing-beat cycles from 10 flies, plotted on a non-dimensional timescale. The instantaneous excitation of the string during the lower reversal of the wing-beat cycle is complemented by a second lift maximum at the beginning of downstroke. (*b*) The aerodynamic force of a pair of wings, calculated according to the quasi-steady aerodynamic theory (same data as in figure 7, average values) fails to account for the measured time course of force generation. (*c*) The inertial force (squares) due to acceleration or deceleration of the wing resembles the measured forces in some aspects. However, these forces do not sustain lift or thrust and do not explain the instantaneous lift pulse at the ventral reversal of the wing beat. The sum of the aerodynamic and inertial forces is shown by the dotted line.

when the wings rotate rapidly between the downstroke and the upstroke ('*quick rotation*') (see paper 1). In the example shown in figure 8*b*, the string is excited to a damped oscillation at roughly the resonance frequency of 3.3 kHz once per wing-beat cycle. This sharp lift pulse is associated with the quick rotation. In addition, a second broader lift maximum (open arrows in figure 8) can be seen roughly half a wing-beat cycle later, apparently at the beginning of downstroke. This less pronounced maximum is more obvious when the noise is reduced in the averaged traces, as can be seen in figure 8*a*, where the signals of 20 wing-beat cycles from the same flight episode were averaged on a non-dimensional timescale, as explained above.

In figure 8(*c*, *d*) the timecourse of the string displacement is shown for two flight episodes from another fly. The string tension was increased, thus changing the resonance frequency from 1.5 kHz (figure 8*c*) to 4.5 kHz (figure 8*d*). Because the wing beat frequency (n_f = 189 Hz) did not change when the string was stressed, it is expected that the instantaneous flight forces might not have changed either. The difference between the two figures is attributed to the effects of string tension. Obviously, there are two major excitations of the string during each wing beat cycle. The first lift pulse associated with the quick wing rotation is sharp enough to induce oscillations at either resonance frequency. The second lift pulse associated with the beginning of the downstroke is comparatively smooth and induces oscillations only at low resonance frequencies (figure 8*c*). When the resonance frequency is sufficiently high (figure 8*d*), the second pulse seems to correspond to the time course of the displacement signal.

The examples shown in figure 8(*b*, *d*) are extreme cases for the ratio between the expression of the first and the second lift maximum. A more representative timecourse of the force

production was obtained by averaging signals of twenty cycles from each of ten flies, plotted on the non-dimensional timescale in figure 9*a*. The mean resonance frequency was 2.5 kHz. The partition into four wing beat phases (upstroke, dorsal reversal, downstroke and ventral reversal) is adopted from the average kinematic data. The relative phase for this 'event scale' is adjusted for the force measurements by using the light barrier signal for stroboscopic inspection of wing posture, as described above. This plot confirms that the sharp lift pulse during the ventral reversal phase is followed by a second, broader and perhaps stronger maximum at the beginning of downstroke, which builds up when the wings perform the squeeze–peel.

4. Discussion

In this second part of the present series of papers, two major results were reported. (i) The average aerodynamic forces calculated according to quasi-steady theory are small compared with the body mass and oriented almost parallel to the longitudinal body axis. As can be easily seen from table 1, this result does not critically depend on the actual boundary conditions of the quasi-steady aerodynamic theory on which the calculations were based. It could be argued that the deficiency in flight force is due to the situation of tethered flight, which might be sensed by the fly. However, the average lift measured for tethered flying *Drosophila melanogaster* (see row 5 in table 1, taken from Götz (1987)) is still conspicuously larger than the calculated time average. Thus, if one excludes the possibility that the flies used for the two sets of experiments differ systematically (female flies of the same wild-type strain and about the same age have been used in these experiments), it can be concluded that the quasi-steady theory fails to explain the essential components of force production in *Drosophila melanogaster*. (ii) The time course of the forces calculated following the quasi-steady assumption differs considerably from the signal of a device designed to assay the instantaneous forces on the fixed flying fly (see figure 9). This result further supports the notion that the quasi-steady theory is inappropriate for the calculation of the flight force of a small insect. Again, the observed discrepancies cannot be due to the situation of tethered flight, because the kinematic and dynamic measurements leading to the different timecourses were obtained under comparable flight conditions. As these measurements might point to alternative aerodynamic mechanisms, such as those proposed by Ellington (1984*d*), the results will be discussed in further detail.

(*a*) *Force measurements*

The major difficulty in interpreting the force measurements is that the actual string displacement is only proportional to the force acting on the string if the string does not start to oscillate. This, however, is not the case; even after damping the string, subcritical oscillations are induced by a sharp impulse, e.g. when a small weight is dropped onto the string. In principle, such difficulties could be overcome by measuring the complete frequency characteristic of the device. However, here only two controls were performed for each flight episode. (i) The sign of force action was confirmed by touching the string with a hair-like wire alternatively from above and from below. (ii) The resonance frequency was crudely estimated from the oscillation induced by dropping a 10 mg weight on the string. Accordingly, the present conclusions from the string measurements are restricted to a more qualitative level.

Despite this restriction, two features can be derived from the average string displacement presented in figure 9*a*. (i) A sharp lift pulse is generated during the ventral reversal of the

wings. (ii) A broad lift maximum is built up during the dorsal reversal. The relation between the magnitude of these two lift peaks varies considerably. The timecourse of the two events differs from force measurements reported by Buckholz (1981) in *Sarcophaga*; he found an almost harmonic oscillation at wing-beat frequency. This discrepancy might be due to interspecific differences or to the fact that his mechanical system was tuned to a resonance frequency close to the wing-beat frequency, which might suppress higher harmonics.

What mechanisms could account for the two lift peaks observed during the wing-beat cycle of *Drosophila*? For direct comparison with the force measurements, in figure 9*b* the timecourse of the quasi-steady aerodynamic force component perpendicular to the average stroke plane, F_s, is plotted on the same timescale. This force component, which is inclined about 40° relative to the longitudinal body axis (see inset, figure 9), would actually be responsible for lift production in a freely hovering fruitfly. Here, a lift maximum is observed during the upstroke and a smaller peak during the downstroke. Most of the time F_s is positive, i.e. almost no force oriented downwards would be generated by a fly hovering with horizontal stroke plane. Because both lift peaks appear later than the measured excitations of the string, and because the lift peak during upstroke is not sharp enough to explain the pulse-like excitation, the measured signal cannot be explained convincingly on the basis of the calculated quasi-steady aerodynamic forces.

So far, we have not considered the *inertial forces* due to the acceleration of the wings and the boundary layer of air around the wings. These forces must be balanced by opposite forces acting on the body of the fly. Although these forces do not produce any net lift, they are picked up by the string. These forces were obtained by multiplying the total mass of the two wings $2m_{wg}$ with the negative acceleration $-dv/dt$ of their centre of gravity. It should be noted that two simplifications are introduced by this method of calculation. (i) It is assumed that the mass distribution is equal on both sides of the axis of supination and pronation. In this case, no inertial forces result from the rotation of the wings around their longitudinal axes. (ii) Concentration of the virtual mass about 2×10^{-5} m distal from the centre of gravity is expected because it increases with the square of wing chord, c^2, instead of with c. Because this difference is small, and the virtual mass is only a small fraction of the total wing mass, this difference was neglected. The time course of the inertial force component perpendicular to the average stroke plane is plotted in figure 9*c*, on the same time scale as the measured forces. Note that the force scale is blown up by a factor of 4, compared with that of the calculated aerodynamic forces in figure 9*b*. The sum of the two forces is shown by the dotted line in figure 9*c*. Surprisingly, even in the direction perpendicular to the average stroke plane, in which the accelerations are expected to be minimal, the inertial forces seem to exceed the aerodynamic forces and are therefore likely to dominate the measured force signal. This appears to be a consequence of the curved trajectory elevating the wing from the average stroke plane during each of the two reversal phases. The peak and the trough of inertial forces during downstroke seem to reflect the measured forces in a first approximation, and the inertial force maximum appears at the same time as the sharp excitation of the string. However, the string does not oscillate upwards and downwards to the same extent, as should be expected from the symmetry of inertial force peak and trough. In contrast, the average level is shifted to higher values, i.e. a net lift is induced. Furthermore, the lift pulse actually generated by the fly seems to be sharper than the inertial force pulse, because the string is excited to oscillations at higher resonant frequencies than those contained in the time course of the inertial force. An additional mechanism seems

PHILOSOPHICAL TRANSACTIONS OF THE ROYAL SOCIETY B BIOLOGICAL SCIENCES

to be required for generating the strong and sharp lift pulse during the ventral reversal phase of the wing beat cycle. This event can neither be explained by the mechanics of wing beat nor by the quasi-steady aerodynamic theory.

When a lift pulse is produced at the end of a half stroke, the flight force does not attach in the centre of gravity of the fly's body. Thus a torque about the transversal body axis is generated which depends on the time course of the flight force. Consequently, the body angle of a free-flying fly should be subjected to a certain oscillation during the wing-beat cycle. As mentioned by Ellington (1984*c*), this could be an indicator for force production in insect flight, if problems of resolution are overcome.

(*b*) *Quasi-steady theory*

What are the possible sources of errors and the restrictions of the aerodynamic calculations done so far? All results derived from equations 1 and 2 depend on the empirical coefficients of lift and drag, C_L and C_D, respectively. Although crudely measured for a small sample of *Drosophila melanogaster* wings, the data are similar to those presented by Vogel (1967) for *Drosophila virilis* (figure 3). According to the results in table 1, the coefficients do not seem to be a major source of errors.

Accurate kinematic data are necessary to calculate the relative velocity and the angle of attack of the wing and, based on these values, the direction and magnitude of the aerodynamic force vector in space. Such data were taken from the kinematic study presented in paper 1 (Zanker 1989*a*). It should be noted that the three-dimensional representation of the wing motion derived here allows the calculation of the quasi-steady force as a vector in space. The kinematic data used here should be fairly representative, because they are based on 1186 single photographs from 10 flies and the s.e.m.s for the kinematic data are considerably small. Artefacts may have been introduced by averaging data from different flies with some error in the relative phase, because high-frequency components are likely to be suppressed under conditions of phase jitter. A strong influence of such errors can be excluded, because control calculations for individual flight episodes, even with extreme deviations from the average kinematics, lead to similar general results. Furthermore, fast transient events of wing-beat kinematics may have been neglected because of the artificially slow sampling rate of the motion pictures, which just gives a time-averaged representation of the wing beat (see paper 1). In a strict sense, only the direct comparison of the wing beat with the force signal from the same fly at the same time, i.e. laser-interferometric measurements combined with simultaneous high-speed microphotography, ensures that the force measurements and aerodynamic calculations correspond to each other. However, it can be argued that artefacts from time-averaging have little influence on the quasi-steady calculations, for two reasons. (i) Transient effects are disregarded by the quasi-steady theory, anyway. (ii) The peak velocities and angles of attack, which lead to the highest contributions to the quasi-steady flight force, appear through comparatively continuous phases of downstroke and upstroke. Under these conditions, phase jitter will have little influence on the magnitude of average data, and the applied procedure should not lead to critical underestimates by quasi-steady aerodynamics.

In contrast to a fixed aerofoil like that of an airplane or a soaring bird, the kinematic variables of an oscillating wing vary considerably from wing base to wing tip. The blade-element theory takes this gradient into account by dissecting the wing into small elements with constant velocity and angle of attack. For each element the lift and drag force component is

PHILOSOPHICAL TRANSACTIONS OF THE ROYAL SOCIETY B BIOLOGICAL SCIENCES

calculated and finally integrated over the whole wing with the chord length of the particular element as weighting factor. The three-dimensional data of wing motion and the shape measurements of *Drosophila* wings presented here were the basis for such calculations. The results in table 1 show that the gain from this approximation is small compared with the overall deficiency in flight forces. No attempt has been made, so far, to account for temporal and spatial modulations of the induced velocity met by the beating wings. The assumption of a constant value of v_{ind} is justified under steady conditions, but appears as an inappropriate simplification in the present case.

To summarize these considerations, the reported discrepancy between measured and calculated flight forces are not due to the limited quality of the measurements, but to violating the restrictions of the theory applied to the data. The calculation of the acting forces according to equations 1 and 2 was based on the assumption that at any time the wing can be treated as moving under steady-state conditions in the air with the instantaneous velocity and angle of attack (quasi-steady assumption). However, this quasi-steady assumption is not met by reality, because the oscillating wing changes its inclination and velocity continuously and rapidly. In general, (i) the single wing cannot be treated independently at two consecutive phase steps, because the circulation of a given phase step depends on the circulation of the wing at the phase steps before; and (ii) the circulation of the two wings of *Drosophila* cannot be treated independently of each other, as they come very close to, or touch, each other during the dorsal reversal. Essential components of spatiotemporal interaction in the dynamics of the wing-beat are obviously not covered by the quasi-steady theory.

(*c*) *Unsteady aerodynamics*

To overcome the shortcomings of the quasi-steady theory, the air flow around the moving wings has to be considered more thoroughly. Aerodynamic theory was substantially expanded by the analysis of unsteady flight mechanisms (see, for example, Weis-Fogh & Jensen 1956; Jensen 1956; Bennett 1970; Weis-Fogh 1973; Maxworthy 1981). These issues are extensively reviewed by Rayner (1979) and Ellington (1984*d*, e) and only a few general points will be mentioned in the following. The flow around a moving aerofoil can formally be decomposed into a pure translational component and a circulation Γ. Using Γ, the lift force acting on a wing element can then be described according to the Kutta–Joukowski theorem as

$$\mathrm{d}L = \rho \Gamma v_{\mathrm{a}} \, \mathrm{d}r. \tag{5}$$

The circulation Γ may result from translational movements of the wing

$$\Gamma_{\mathrm{t}} = \tfrac{1}{2}(c v_{\mathrm{a}} C_{\mathrm{L}}), \tag{6}$$

which transforms equation 5 into an expression analogous to equation 1. In addition, rotational wing movements lead to a circulation not covered by the quasi-steady theory so far, which can be expressed as

$$\Gamma_{\sigma} = \gamma(\mathrm{d}\alpha_{\mathrm{m}}/\mathrm{d}t)\, c^2, \tag{7}$$

where γ is the rotational lift coefficient. As long as rotational and translational speeds do not change, the lift can be directly calculated from equations 5–7. However, during the wing-beat cycle of *Drosophila*, for instance, both translational and rotational speeds vary periodically, i.e. the circulation around the wing is modified continuously. This complicates the flow situation in two major aspects. (i) According to Kelvin's circulation theorem, any change of circulation

$d\Gamma$ is accompanied by the generation of a complementary circulation $-d\Gamma$, which is shed into the wake as a vortex. The vortex sheet shed during wing oscillation convects downwards, leading to additional velocity components and changes of the wing's angle of attack. Accordingly, the total circulation Γ satisfying the Kutta condition in equation 5 is formally extended by the circulation of wake vorticity Γ_i. (ii) The growth of circulation around a section does not follow immediately the timecourse of velocity and angle of attack, as should be expected from equations 6 and 7: even when a wing has travelled six chord lengths after the onset of translational motion, circulation and lift are only about 90% of the quasi-steady values. This so-called 'Wagner effect' reflects the delay of vortex shedding into the wake.

Estimating the lift forces from the circulation enables two approaches. (i) Lift can be deduced from the pattern of air flow which was visualized by suitable techniques (see, for example, Maxworthy 1979; Speeding *et al.* 1984). (ii) The 'vortex theory' of hovering flight (Ellington 1984*e*,*f*) combines the momentum and the circulation approach to flapping flight aerodynamics, leading to the concept of a 'pulsed actuator disc'. This concept invokes two correction factors for the Rankine–Froude estimate of induced power, P^*_{RF}, one spatial (σ) regarding the inhomogeneity of circulation over the wing-stroke area, the other temporal (τ) referring to the variation of circulation throughout the oscillation cycle. This leads to formulae for the mean power required to overcome profile drag ($\overline{P^*_{pro}}$), to accelerate the surrounding air by means of quasi-steady ($\overline{P^*_{ind}}(C_L)$) or rotational ($\overline{P^*_{ind}}(\gamma)$) mechanisms and to overcome the inertia of the wings ($\overline{P^*_{acc}}$). By equating the weight and the circulatory lift for a hovering animal, the following coefficients can be derived: (i) the mean lift coefficient $\overline{C_L}$, which is sufficient to explain hovering flight by quasi-steady mechanisms; and (ii) the mean rotational lift coefficient $\bar{\gamma}$, which is a measure for the relative strength of (unsteady) rotational mechanisms involved in lift production. Some of the aerodynamic parameters calculated from our kinematic data according to Ellington's vortex theory are shown in table 2. The corresponding values for male fruitflies (taken from Laurie-Ahlberg *et al.* 1985) and the hoverfly *Episyrphus* (taken from Ellington 1984*f*) are listed for comparison. Before discussing the parameters in detail, one should remember that the vortex theory relies on assumptions about wing-beat kinematics to ease the calculations. One prominent approximation, which holds quite well for the species investigated by Ellington (1984*c*), is that of harmonic wing oscillation. However, this is not the case for *Drosophila*, as can be seen in figure 5 from the peak values of the wing speed, or from the deviation of the actual ratio (1.4) of the duration of downstroke and upstroke from the ratio $d/u = 1.0$ expected in harmonic oscillation.

The mean lift and drag coefficients calculated according to the vortex theory differ considerably between the two fly species in table 2. Owing to the smaller Reynolds number the *mean profile drag coefficient* $\overline{C_{D,pro}} = 0.59$ of the fruitfly exceeds that of the hoverfly. However, this value roughly corresponds to aerodynamic angles of attack of about 30°, which is about the mean inclination of the wing actually observed during translation. This is to say that Ellington's estimate of $\overline{C_{D,pro}}$ seems to hold even for small insects like *Drosophila*. The *mean quasi-steady lift coefficient* required to keep the fly airborne, $\overline{C_L} = 0.62$, is much smaller than that of *Episyrphus*, mainly because of the assumed value of the mean lift $\overline{L^*} = 0.41$ in units of the body weight. When the fly has to lift the complete body weight (not the case in tethered flight; see Götz (1987), $\overline{L^*}$ is by definition 1.0 and $\overline{C_L}$ must be 1.45, if the wing beat is not changed. One important point should be noted here. Because the value of $\overline{C_L} = 0.62$ is comparatively small and close to the values actually measured for *Drosophila* wings at angles of

TABLE 2. AERODYNAMIC PARAMETERS CALCULATED ACCORDING TO ELLINGTON'S VORTEX THEORY

(The profile power, induced power and, in the absence of elastic storage, inertial power contribute to mechanical power output: $P_m = P_{pro} + P_{ind} + P_{acc}$. The asterisk (*) denotes the specific power components per unit weight supported (dimension W N^{-1}); the bars ($\bar{}$) relate to averages for a wing-beat cycle.)

parameter		*Episyrphus* (free flight) (Ellington 1984*d*)	*Drosophila* (tethered flight) (present study)		*Drosophila* (tethered flight) (Laurue-Ahlberg *et al.* 1985)
mean lift in units of body weight	$\overline{L^*}$	1.00	0.41	(1.00)	1.00
mean profile drag coefficient	$\overline{C_{D,pro}}$	0.26	0.59	—	0.78
mean lift coefficient	$\overline{C_L}$	1.17	0.62	(1.45)	—
mean rotational life coefficient	γ	0.41	0.31–0.57	(0.75–1.36)	—
temporal correction factor	τ	0.05	0.046	(0.113)	—
quasi-steady spatial correction factor	$\sigma(C_L)$	0.07	0.14	—	—
rotational spatial correction factor	$\sigma(\gamma)$	0.09	0.09	—	—
mean specific profile power	$\overline{P^*_{pro}}$	0.96	1.06	—	0.79
mean specific quasi-steady induced power	$\overline{P^*_{ind}}(C_L)$	0.90	0.160	(0.64)	0.64
mean specific rotational induced power	$\overline{P^*_{ind}}(\gamma)$	1.00	0.153	(0.62)	0.64
mean specific inertial power	$\overline{P^*_{acc}}$	6.44	5.80	—	1.91

attack between 30° and 60°, this result would not have led to the rejection of the quasi-steady assumption in former investigations (see, for example, Weis-Fogh 1973). However, in the present study it was shown that despite the moderate mean lift coefficient necessary to allow hovering flight, the quasi-steady assumption is definitely not justified. Even if the reduction of mean lift in tethered flight is taken into account, the lift produced according to this theory is not sufficient. The *mean rotational lift coefficient* $\bar{\gamma}$ is a measure for the amount of circulation which has to be induced by rotational wing movements if the fly was lifted by such mechanisms. For *Drosophila*, a value between 0.57 and 0.31 is derived (1.36 and 0.75 if lift of the body weight is assumed), depending on the mean rotational speed which was either (i) calculated as the average for the complete pronation and supination phase (5.5 rad per wing-beat cycle) or (ii) was corrected to a more realistic value of 10 rad per cycle, when only the time intervals of strong rotations were considered. For both conditions, the values of $\bar{\gamma}$ are similar for *Drosophila* and *Episyrphus*, but small compared with the estimate derived, for instance, from theoretical and model investigations (see Ellington 1984*f*) for the clap–fling mechanism. Accordingly, the fly should be able to lift its body weight based on rotational mechanisms.

From the parameters calculated so far, the specific power requirements, i.e. the power needed to lift a unit of body weight, are derived. The Rankine–Froude estimate of mean specific induced power P^*_{RF} is corrected for spatial inhomogeneity and periodicity of the wake produced by the pulsed actuator disc, by the spatial factor σ and the temporal factor τ. In *Drosophila* the quasi-steady spatial correction factor tends to be greater than in *Episyrphus*, i.e. the energy loss by spatial variation of wake velocity is increased. This is probably due to the less harmonic wing motion of the fruitfly. The resulting values for the *quasi-steady and rotational induced power* of *Drosophila*, $\overline{P^*_{ind}}(C_L)$ and $\overline{P^*_{ind}}(\gamma)$, are low compared with those of *Episyrphus*, because the Rankine–Froude estimate ($P^*_{RF} = 0.14$ W N^{-1}, not listed in table 2) is far below that of

Episyrphus (about 0.9) owing to the smaller wing loading of *Drosophila*. Because the values for quasi-steady and rotational mechanisms are almost the same, the energy consumption does not seem to depend critically on the involved aerodynamic mechanism. This simplifies the evaluation of the specific aerodynamic power, $\overline{P^*_a} = 1.20$, which is the sum of profile power and induced power. Because the mean specific profile power is about the same for both species, whereas the Rankine–Froude estimate differs considerably, the *aerodynamic efficiency*, $\eta_a = P^*_{RF}/\overline{P^*_a} = 0.11$, is smaller in *Drosophila* than in *Episyrphus* (0.45). This low value reflects the decrease of aerodynamic efficiency in the range of low Reynolds numbers, when the importance to profile drag increases compared with the other aerodynamic forces. Finally, the mean power output per unit mass of flight muscles $\overline{P^*_m}$ and the *mechanochemical efficiency* η_m (i.e. the ratio between power output and energy consumption) are calculated from the mean metabolic power input of about 18 W N^{-1} (Götz 1987) during tethered flight. To find the upper and lower limit, two assumptions were used. (i) The wings have to be accelerated actively by the muscles requiring the mean specific $\overline{P^*_{acc}}$, in addition. (ii) The kinetic energy of the wing beat is completely stored in elastic elements when the wings are decelerating at the end of each halfstroke ($\overline{P^*_{acc}} = 0$). Both values of mean muscular power output $\overline{P^*_m}$ (22 and 7.5 W N^{-1}, respectively) are compatible with a maximum of about 30 W N^{-1}, as suggested for asynchronous fibrillar flight muscles in insects (Ellington 1985, for example). On the other hand, unexpectedly high mechanochemical efficiencies (0.20 instead of 0.068) are the result of assuming the absence of elastic storage. Thus it seems realistic to expect at least partial storage of kinetic energy in elastic elements. All these values differ slightly from those calculated by Laurie-Ahlberg *et al.* (1985), who used male flies, which are generally smaller than females, did not correct for reduced lift production in tethered flight, and assumed harmonic oscillation of the wings.

The comparison of the mean lift coefficients $\overline{C_L}$ and $\bar{\gamma}$ shows that quasi-steady mechanisms are unlikely to account for lift production in hovering *Drosophila*, whereas rotational mechanisms could easily generate sufficient lift. Which wing rotations could be responsible for this mechanism? The two phases of reversal between the half strokes are the likely candidates already discussed above. Inspired by the unsteady aerofoil theory, the clap–fling of small insects (Weis-Fogh 1973; Bennett 1977) has been interpreted as an elaborate mechanism to reduce the Wagner effect. The stop vortex of one wing is the start vortex of the other and vice versa, and therefore the circulation is reduced at the end of upstroke and built up immediately at the beginning of downstroke. Thus, losses due to vortex shedding are prevented (Lighthill 1973; Maxworthy 1981). This event seems to contribute to the lift maximum observed at the beginning of the downstroke in the force measurements presented here.

Compared with the extensively investigated clap–fling, the events during the ventral reversal phase of wing beat have found only little interest, so far. The discrepancy between the measured forces and the forces expected under quasi-steady conditions indicate that during this phase unsteady effects should play an important role in lift production. Because the circulation around the wing must change its sign between downstroke and upstroke, shedding or mutual exchange of a combined start- and stop-vortex is expected at just this moment. Owing to the Wagner effect, conventional vortex shedding will reduce the production of circulatory lift. A hypothetical 'flex mechanism' was proposed by Ellington (1984*d*) to accelerate vortex shedding during isolated rotation, thus decreasing the influence of the Wagner effect. In addition, it might be speculated that the extremely rapid wing rotation could facilitate the

shedding of the combined start- and stop-vortices and impart a strong downward momentum to this vortex. This could be used by the fly to gain lift from the conservation of the overall momentum (Ellington 1984*e*). The 'fast supination effect' discussed by Nachtigall (1979) for *Phormia* resembles this mechanism, at first glance. However, supination in the blowfly is far less pronounced than in *Drosophila*; in addition, the vortex separated from the trailing edge of the wing in Nachtigall's (1979) sketch seems to move in a direction unlikely to support lift. The present conjectures have to be corroborated by future research. Flow visualization (Maxworthy 1981) is obviously not a simple task for the tiny fruitfly. However, this might help to discriminate between assumed and actual flight mechanisms. The investigation of these mechanisms under conditions of free flight will be another goal for the future.

In conclusion, the flight of *Drosophila melanogaster* is likely to depend for a major part on unsteady effects. By clever exploitation of the necessarily unsteady aerodynamics at high wing-beat frequencies, the small fly has learned to cope with the disadvantage of low Reynolds numbers and the lack of conventional aerofoil action.

We thank A. Borst, M. Egelhaaf and G. Mohn for carefully reading earlier versions of the manuscript; B. Bochenek for preparing the figures; and U. Flaiz for typing the manuscript. This work was supported by a grant from the M.P.G.

References

Alexander, R. McN. & Goldspink, G. 1977 *Mechanics and energetics of animal locomotion*. New York: John Wiley.
Bennett, L. 1970 Insect flight: lift and rate of change of incidence. *Science, Wash.* **167**, 177–179.
Bennett, L. 1973 Effectiveness and flight of small insects. *Ann. ent. Soc. Am.* **66**, 1187–1190.
Bennett, L. 1977 Clap and fling aerodynamics – an experimental evaluation. *J. exp. Biol.* **69**, 261–272.
Buckholz, R. H. 1981 Measurements of unsteady periodic forces generated by the blowfly flying in a wind tunnel. *J. exp. Biol.* **90**, 163–173.
Cloupeau, M., Devillers, J. F. & Devezeaux, D. 1979 Direct measurements of instantaneous lift in desert locust; comparison with Jensen's experiments on detached wings. *J. exp. Biol.* **80**, 1–15.
Curtsinger, J. W. & Laurie-Ahlberg, C. C. 1981 Genetic variability of flight metabolism in *Drosophila melanogaster*. I. Characterization of power output during tethered flight. *Genetics* **98**, 549–564.
David, C. T. 1978 The relationship between body angle and flight speed in free-flying *Drosophila*. *Physiol. Ent.* **3**, 191–195.
Ellington, C. P. 1984*a* The aerodynamics of hovering insect flight. I. The quasi-steady analysis. *Phil. Trans. R. Soc. Lond.* B **305**, 1–15.
Ellington, C. P. 1984*b* The aerodynamics of hovering insect flight. II. Morphological parameters. *Phil. Trans. R. Soc. Lond.* B **305**, 17–40.
Ellington, C. P. 1984*c* The aerodynamics of hovering insect flight. III. Kinematics. *Phil. Trans. R. Soc. Lond.* B **305**, 41–78.
Ellington, C. P. 1984*d* The aerodynamics of hovering insect flight. IV. Aerodynamic mechanisms. *Phil. Trans. R. Soc. Lond.* B **305**, 79–113.
Ellington, C. P. 1984*e* The aerodynamics of hovering insect flight. V. A. vortex theory. *Phil. Trans. R. Soc. Lond.* B **305**, 115–144.
Ellington, C. P. 1984*f* The aerodynamics of hovering insect flight. VI. Lift and power requirements. *Phil. Trans. R. Soc. Lond.* B **305**, 145–181.
Ellington, C. P. 1985 Power and efficiency of insect flight muscle. *J. exp. Biol.* **115**, 293–304.
Götz, K. G. 1968 Flight control in *Drosophila* by visual perception of motion. *Kybernetik* **4**, 199–208.
Götz, K. G. 1987 Course-control, metabolism and wing inference during ultralong tethered flight in *Drosophila melanogaster*. *J. exp. Biol.* **128**, 35–46.
Götz, K. G. & Wandel, U. 1984 Optomotor control of the force of flight in *Drosophila* and *Musca*. II. Covariance of lift and thrust in still air. *Biol. Cybern.* **51**, 135–139.
Hollick, F. S. J. 1940 The flight of the dipterious fly *Muscina stabulans* Fallén. *Phil. Trans. R. Soc. Lond.* B **230**, 357–390.
Horridge, G. A. 1956 The flight of very small insects. *Nature, Lond.* **178**, 1334–1335.

PHILOSOPHICAL TRANSACTIONS OF THE ROYAL SOCIETY B BIOLOGICAL SCIENCES

Jensen, M. 1956 Biology and physics of locust flight. III. The aerodynamics of locust flight. *Phil. Trans. R. Soc. Lond.* B **239**, 511–552.

Laurie-Ahlberg, C. C., Barnes, P. T., Curtsinger, J. W., Emigh, T. H., Karlin, B., Morris, R., Norman, R. A. & Wilton, A. N. 1985 Genetic variability of flight metabolism in *Drosophila melanogaster*. II. Relationship between power output and enzyme activity levels. *Genetics* **111**, 845–868.

Lighthill, M. J. 1973 On the Weis-Fogh mechanism of lift generation. *J. Fluid Mech.* **60**, 1–17.

Maxworthy, T. 1979 Experiments on the Weis-Fogh mechanism of lift generation by insects in hovering flight. I. Dynamics of the 'fling'. *J. Fluid. Mech.* **93**: 47–63.

Maxworthy, T. 1981 The fluid dynamics of insect flight. *A. Rev. Fluid Mech.* **13**, 329–350.

Nachtigall, W. 1966 Die Kinematik der Schlagflügelbewegungen von Dipteren. Methodische und analytische Grundlagen zur Biophysik des Insektenflugs. *Z. vergl. Physiol.* **52**, 155–211.

Nachtigall, W. 1979 Rasche Richtungsänderungen und Torsionen schwingender Fliegenflügel und Hypothesen über zugeordnete instationäre Strömungseffekte. *J. comp. Physiol.* **133**, 351–355.

Nachtigall, W. & Roth, W. 1983 Correlations between stationary measurable parameters of wing movement and aerodynamic force production in the blowfly (*Calliphora vicine* R.-D.). *J. comp. Physiol.* **150**, 251–260.

Osborne, M. F. M. 1951 Aerodynamics of flapping flight with application to insects. *J. exp. Biol.* **28**, 221–245.

Rayner, J. M. V. 1979 A new approach to animal flight mechanisms. *J. exp. Biol.* **80**, 17–54.

Spedding, G. R., Rayner, J. M. V. & Pennycuick, C. J. 1984 Momentum and energy in the wake of a pigeon (*Columba livia*) in slow flight. *J. exp. Biol.* **111**, 81–102.

Thom, A. & Swart, P. 1940 The forces on an aerofoil at very low speeds. *Jl R. Aeronaut. Soc.* **44**, 761–770.

Vogel, S. 1966 Flight in *Drosophila*. I. Flight performance of tethered flies. *J. exp. Biol.* **44**, 567–578.

Vogel, S. 1967 Flight in *Drosophila*. III. Aerodynamic characteristics of fly wings and wing models. *J. exp. Biol.* **46**, 431–443.

Vogel, S. 1981 *Life in moving fluids. The physical biology flow*. New Jersey: Princeton University Press.

Weis-Fogh, T. 1956 Biology and physics of locust flight. II. Flight performance of the desert locust (*Schistocerca gregaria*). *Phil. Trans. R. Soc. Lond.* B **239**, 459–510.

Weis-Fogh, T. & Jensen, M. 1956 Biology and physics of locust flight. I. Basic principles in insect flight. A critical review. *Phil. Trans. R. Soc. Lond.* B **239**, 415–458.

Weis-Fogh, T. 1972 Energetics of hovering flight in hummingbirds and in *Drosophila*. *J. exp. Biol.* **56**, 79–104.

Weis-Fogh, T. 1973 Quick estimates of flight fitness in hovering animals, including novel mechanisms for lift production. *J. exp. Biol.* **59**, 169–230.

Wood, J. 1970 A study of the instantaneous air velocities in a plane behind the wings of certain diptera flying in a wild tunnel. *J. exp. Biol.* **52**, 17–25.

Zanker, J. M. 1988 On the mechanism of speed- and altitude-control in *Drosophila melanogaster*. *Physiol. Entomol.* **13**, 351–361.

Zanker, J. M. 1990*a* The wing beat of *Drosophila melanogaster*. I. Kinematics. *Phil. Trans. R. Soc. Lond.* B **327**, 1–18. (Preceding paper.)

Zanker, J. M. 1990*b* The wing beat of *Drosophila melanogaster*. III. Control. *Phil. Trans. R. Soc. Lond.* B **327**, 45–64. (Following paper.)

Zarnack, W. 1969 Kinematik der Flügelschlagbewegungen bei *Locusta migratoria* L. Dissertation, Ludwig-Maximilans-Universität, München.

PHILOSOPHICAL TRANSACTIONS OF THE ROYAL SOCIETY B BIOLOGICAL SCIENCES